Showcasing research from Professor Okubo's laboratory, Department of Chemical System Engineering, School of Engineering, The University of Tokyo, Japan.

Tracking the rearrangement of atomic configurations during the conversion of FAU zeolite to CHA zeolite

Understanding formation mechanisms at the atomic scale is essential toward the rational design and synthesis of zeolites; still, it remains challenging because of the unknown atomic configurations of starting and intermediate species. K. Muraoka, Y. Sada, A. Shimojima, W. Chaikittisilp, and T. Okubo combine NMR techniques with high-throughput computational calculations to understand how atomic configurations change when CHA zeolite is crystallized from FAU zeolite. Despite their structural similarity, the conversion involves significant atomic rearrangement, which can be explained by the substitution of Al for Si within their common structural building unit—a prism break.

ROYAL SOCIETY OF CHEMISTRY | Celebrating IYPT 2019

rsc.li/chemical-science

Tracking the rearrangement of atomic configurations during the conversion of FAU zeolite to CHA zeolite†

Koki Muraoka, [iD] ‡§[a] Yuki Sada, [iD] ‡[a] Atsushi Shimojima, [iD] [bc]
Watcharop Chaikittisilp [iD] [d] and Tatsuya Okubo [iD] *[a]

In order to realize designed synthesis, understanding the formation mechanism of zeolites at an atomic level has long been aspired, but remains challenging due to the fact that the knowledge of atomic configurations of the species formed during the process is limited. We focus on a synthesis system that crystallizes CHA zeolite from FAU zeolite as the sole source of tetrahedral atoms of Si and Al, so that end-to-end characterization can be conducted. Solid-state ^{29}Si MAS NMR is followed by high-throughput computational modeling to understand how atomic configurations changed during the interzeolite conversion. This reveals that the structural motif commonly found in FAU and CHA is not preserved during the conversion; rather, there is a specific rearrangement of silicates and aluminates within the motif. The atomic configuration of CHA seems to be influenced by that of the starting FAU, considering that CHA synthesized without using FAU results in a random Al distribution. A Metropolis Monte-Carlo simulation combined with a lattice minimization technique reveals that CHA derived from FAU has energetically favorable, biased atomic locations, which could be a result of the atomic configurations of the starting FAU. These results suggest that by choosing the appropriate reactant, Al placement could be designed to enhance the targeted properties of zeolites for catalysis and adsorption.

Introduction

Understanding formation mechanisms at an atomic scale is essential for the rational design and synthesis of materials. Once established, this approach should be able to identify fundamental factors in controlling materials formation as well as the corresponding process parameters, ultimately enabling the synthesis of novel materials with desired and adjustable properties. This approach has been extensively used in organic synthesis to connect building blocks and has produced countless numbers of chemical entities.[1,2] Although atomic-level understanding has been aspired to for years with zeolite synthesis,[3] previous studies have been limited owing to the nature of hydrothermal synthesis, which is a standard technique to prepare these microporous materials. The reaction is generally mediated by amorphous aluminosilicates,[4–8] which makes the elucidation of the formation mechanism difficult. *In situ* analyses of zeolite formation[9–15] have been conducted to capture a detailed image of zeolite synthesis. Although these studies have deepened our understanding of the mechanism, the exact atomic rearrangement during this process is unknown, which makes it fundamentally challenging to link intermediate species with the formed zeolite structures.

Atomic-level understanding has not even been achieved for the zeolite product itself. Zeolites are crystalline microporous materials built from tetrahedral atoms and bridging oxygen atoms. Depending on the topology of the chemical network, different three-letter codes are assigned, such as **FAU** and **CHA**. While it has been well accepted that Si or Al can occupy the tetrahedral sites of aluminosilicate zeolites, conventional diffraction techniques can hardly differentiate Si and Al; hence, the precise atomic arrangements of Si and Al within zeolites were barely understood until very recently.[16] Current progress in characterization techniques, detailed catalytic studies, and

[a]*Department of Chemical System Engineering, The University of Tokyo, 7-3-1 Hongo, Bunkyo-ku, Tokyo 113-8656, Japan. E-mail: okubo@chemsys.t.u-tokyo.ac.jp*

[b]*Department of Applied Chemistry, Waseda University, 3-4-1 Ohkubo, Shinjuku-ku, Tokyo 169-8555, Japan*

[c]*Kagami Memorial Research Institute for Materials Science and Technology, Waseda University, 2-8-26 Nishiwaseda, Shinjuku-ku, Tokyo 169-0051, Japan*

[d]*Research and Services Division of Materials Data and Integrated System (MaDIS), National Institute for Materials Science (NIMS), 1-1 Namiki, Tsukuba, Ibaraki 305-0044, Japan*

† Electronic supplementary information (ESI) available: SEM images, crystal structures closest to ^{29}Si MAS NMR spectra, complete relationship of *d6r* species, fraction of *d6r* species, and an XRD pattern of a control experiment. See DOI: 10.1039/c9sc02773d

‡ These authors contributed equally.

§ Present address: Energy Technologies Area, Lawrence Berkeley National Laboratory, Berkeley, CA 94720, USA.
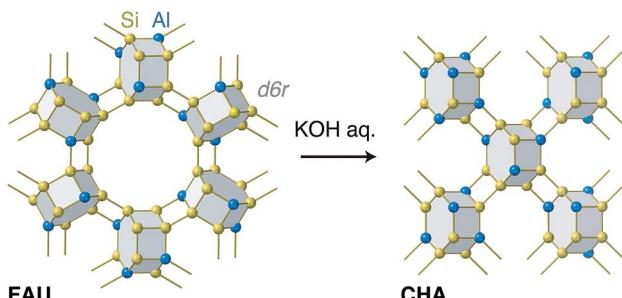
Fig. 1 A schematic illustration of interzeolite conversion from **FAU** to **CHA** in the presence of a KOH aqueous solution without any additional Si or Al sources. Both **FAU** and **CHA** are constructed with a building unit, *d6r* (grey hexagonal prism). Yellow spheres are Si atoms, light blue spheres are Al atoms, and the yellow sticks are O atoms.

theoretical studies have enabled the quantification of the location of Al in zeolites.[17–26]

Because the detailed structures of some zeolites have been studied extensively, employing them as a seed crystal in starting materials is an effective means to deduce zeolite formation mechanisms.[27–29] Indeed, seed-directed zeolite syntheses by the authors have shown structural similarities between the seeds and products, implying that the atomic structures of aluminosilicate species formed before the completion of zeolite growth can influence the structure of the zeolite products.[28] However, seed-directed methods generally entail additional Si and Al sources in the starting materials, which complicates the formation mechanism and makes it difficult to understand.

In this sense, zeolite synthesis using another zeolite as the sole Si and Al source—the so-called "true interzeolite conversion (IZC)"[30]—is an attractive system to study, because the atomic-level structural information for the reactant and product is available. As is the case with seed-directed methods, several studies have discussed the structural similarity in IZC. A previous study assessed IZC from *BEA to MFI and claimed that their common building unit, termed *mor*, played an important role during the synthesis.[31] In addition to other studies emphasizing common structural motifs in IZC,[32,33] Martín *et al.* noted the possibility that **FAU** in reactant mixtures supplies a building unit, termed a double-six-ring (*d6r*), to foster the formation of **CHA**.[34] Interestingly, both **FAU** and **CHA** are solely constructed with *d6r* as shown in Fig. 1, although there is no evidence to prove that *d6r* in **FAU** is directly transferred to **CHA** with the chemical topology intact.[35] Another interesting point is that true IZC generally proceeds without the formation of amorphous matter,[30] implying that end-to-end solid characterization is achievable. These features motivated us to examine the atomic configuration of **CHA** synthesized from **FAU** without any additional Si or Al sources. The combined experimental and computational analyses showed that **CHA** derived from IZC had a biased, energetically favorable atomic configuration, which could be the result of the atomic configuration of the starting **FAU**, although the *d6r* structure did not remain intact during the conversion.

Methods

Synthesis of zeolites

The starting Na-type **FAU** zeolite (HSZ-320NAA, Si/Al = 2.69) was purchased from Tosoh Corporation. Potassium chloride (99.9%) and potassium hydroxide (85%) were purchased from FUJIFILM Wako Pure Chemical Corporation. Ludox AS-40 colloidal silica (40%) and aluminum hydroxide were purchased from Sigma Aldrich. 1 g of the starting Na-type **FAU** and 4 g of potassium chloride were dispersed in 80 g of deionized water and agitated at 333 K for 2 h. The solid sample was recovered *via* filtration and thoroughly washed using deionized water. This ion-exchange procedure was repeated three times. The solid product was dispersed in a potassium hydroxide aqueous solution. This mixture had a chemical composition of 2.7 SiO_2 : 1.0 $Al(OH)_3$: 2.2 KOH : 150H_2O, and was heated at 423 K under autogenous pressure for 110 h in a Teflon reactor encapsulated in a stainless-steel autoclave tumbled at 20 rpm. The solid sample was recovered *via* filtration, thoroughly washed using deionized water, and dried at 353 K. For a control experiment, aluminum hydroxide was dissolved in a potassium hydroxide aqueous solution. After obtaining a clear colorless solution, colloidal silica was slowly added. The resulting mixture was agitated at ambient temperature and transferred to the Teflon reactor. The same heating and recovering procedures were applied.

Characterization

Powder X-ray diffraction (XRD) patterns were recorded on a diffractometer with CuKα radiation (λ = 1.54056 Å, Rigaku Ultima IV, 40 kV, 40 mA) at a scanning rate of 4° min^{-1} over a range of 3° to 50°. Thermogravimetric analyses were performed on a PU 4K (Rigaku) with a heating rate of 10 K min^{-1}, using a mixture of 10% O_2 and 90% He as the carrier gas. Samples dissolved in hydrofluoric acid were characterized using an inductively coupled plasma-atomic emission spectrometer (iCAP-6300, Thermo Scientific). Solid-state NMR spectra were recorded on a JEOL JNM ECA-400 spectrometer. ^{27}Al magic-angle spinning (MAS) NMR spectra were recorded at 104.17 MHz with a relaxation delay of 1 s (30° pulse). ^{29}Si MAS NMR spectra were recorded at 79.42 MHz with a relaxation delay of 100 s (45° pulse). Peak areas of the ^{29}Si MAS NMR spectra were deconvoluted with Voigt functions using dmfit software.[36] A field emission scanning electron microscope (SEM, Hitachi S-4700) was used for characterizing the morphology of the solid samples.

Computation

Crystal structures of **FAU** and **CHA** were obtained from a database.[37] After discarding crystal symmetries, crystal models of **FAU** with the chemical composition $Si_{140}Al_{52}O_{384}$ (Si/Al = 2.69), without any Al–O–Al moieties, were generated by randomly introducing Al following a specific computational protocol.[23,38] Models for **CHA** having the chemical composition $Si_{198}Al_{90}O_{576}$ (Si/Al = 2.20) were created using the same procedure after expanding the unit cell by 2 × 2 × 2. The models closest to the

experimental observations were identified using a method reported previously.[23] Our in-house code was used to analyze the fraction of $Q^4(n\mathrm{Al})$ species. Models for **CHA** synthesized without using **FAU** were built through the same procedure with the reported chemical composition $\mathrm{Si_{207}Al_{81}O_{576}}$ (Si/Al = 2.56). The difference between the crystal models and experimentally observed $^{29}\mathrm{Si}$ MAS NMR spectra was defined as follows.

$$\mathrm{Difference} = \sum_{n=0}^{4} |F_{\mathrm{NMR}}(n\mathrm{Al}) - F_{\mathrm{Model}}(n\mathrm{Al})|$$

$F_{\mathrm{NMR}}(n\mathrm{Al})$ is the fraction of $Q^4(n\mathrm{Al})$ species by $^{29}\mathrm{Si}$ MAS NMR, while $F_{\mathrm{Model}}(n\mathrm{Al})$ is that derived from the modeling.

A Metropolis Monte-Carlo scheme was implemented and utilized based on the GULP package.[39] Initial locations of counter cations were randomly decided based on geometrical considerations.[23,38] After two counter cations were randomly selected, they were relocated based on randomly assigned oxygen atoms and the corresponding geometrical relations.[23,38] After performing lattice minimization under constant pressure for 10 steps using a force field;[40] this swapping was accepted if either the energy decreased, or with a probability of $P = \exp(-\Delta E/k_\mathrm{B}T)$ if the energy increased. ΔE is the energy difference, k_B is the Boltzman constant, and the temperature (T) was 423 K. After repeating the swapping 800 times, the final structure was optimized up to 1000 steps. Potassium cations were used for **CHA**, while sodium cations were used for **FAU**. Ten models with random Al distributions underwent the same Metropolis Monte-Carlo simulation for each case.

Results and discussion

In conventional **FAU**-to-**CHA** conversion, dealuminated **FAU** with many defects[41] in the framework is frequently employed;[32,34,42] still, it is not desirable for analyzing atomic configurations.[23] Here, we started with Al-rich **FAU** to crystallize **CHA** in a KOH aqueous solution without any organics as shown in Fig. 1. The XRD patterns in Fig. 2 show that the peaks resulting from **FAU** decrease as the diffraction derived from **CHA** increases, as the hydrothermal treatment progresses.
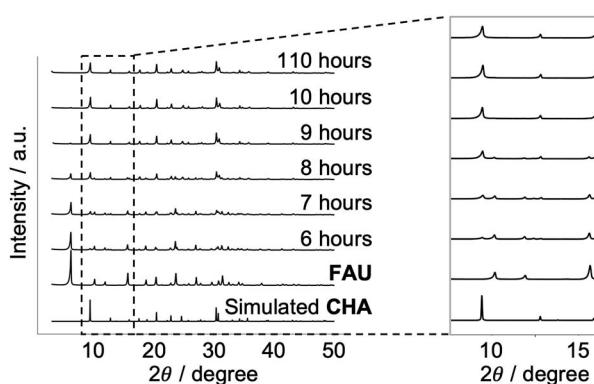

Fig. 2 Powder X-ray diffraction patterns of the starting **FAU** and recovered samples with different heating times together with the simulated patterns for **CHA**.

After 110 hours, all **FAU** was completely consumed and fully crystallized **CHA** was obtained. By examining the XRD patterns (Fig. 2) and SEM images (Fig. S1†), no amorphous matter can be observed throughout the conversion process, which is a common occurrence in other IZC systems,[30] although the resolution of these techniques cannot confirm complete absence. Elemental analysis showed that the Si/Al molar ratio decreased from 2.69 to 2.17 *via* the **FAU**-to-**CHA** conversion. The decrease in Si/Al under alkaline synthesis conditions is a common phenomenon because the Si–O–Si bond is more easily cleaved by hydroxyl ions than the Si–O–Al bond.[43] Such a change in the chemical composition is one of the possible factors that drive the conversion. Another plausible driving force in IZC is the formation of zeolites with a higher framework density,[44,45] which holds for the conversion of **FAU** with a framework density of 13.3 T nm^{-3} to **CHA** with a framework density of 15.1 T nm^{-3}.[37]

The peaks centered at approximately 60 ppm in the $^{27}\mathrm{Al}$ NMR spectra of **FAU** and **CHA** indicated that all Al species were incorporated into the zeolite frameworks with tetrahedral coordination (Fig. S2†), which is consistent with the high crystallinity of both zeolites. Because **FAU** and **CHA** have only one crystallographic tetrahedral site each, highly symmetric and sharp peaks were observed. The fact that **FAU** and **CHA** have only one crystallographic tetrahedral site is advantageous for analyses using $^{29}\mathrm{Si}$ MAS NMR.[23] It is well accepted, particularly for zeolites with a single crystallographic tetrahedral site, that peaks in the $^{29}\mathrm{Si}$ MAS NMR spectra are ascribed to Si(–O–Si)$_{4-n}$(–O–Al)$_n$, *i.e.* $Q^4(n\mathrm{Al})$ species. From the peak areas in the $^{29}\mathrm{Si}$ MAS NMR spectra (Fig. 3a and e), the Si/Al ratios in the frameworks of **FAU** and **CHA** were calculated to be 2.74 and 2.20, respectively. These values are remarkably consistent with those from elemental analyses, presumably owing to the scarcity of defects (*i.e.*, Q^3; Si(–O–H)(–O–Si)$_{3-n}$(–O–Al)$_n$, n = 0–3) as confirmed from the NMR spectra. This is also supported by the crystal shapes and sizes (Fig. S1†).

To obtain the possible atomic configurations, we employed previously reported methods[25] to compute 10 000 aluminosilicate models for both **FAU** and **CHA** with the observed respective chemical compositions, but with random Al distributions.[25] We then calculated the fraction of $Q^4(n\mathrm{Al})$ for each crystalline model and compared it to the experimentally observed values. As shown in Fig. 3b and f, this comparison shows that experimental values of both the starting **FAU** and resulting **CHA** were not statistically average but biased, as observed for siliceous **FAU** obtained *via* direct synthesis.[23] The statistical plots in Fig. 3c and g confirm this, as the experimental values are within the range of outliers for both cases. For comparison, we performed the same computational analyses for **CHA** with similar Si/Al values, synthesized by hydrothermally treating a mixture of colloidal silica, aluminum hydroxide, potassium hydroxide, and water with the chemical composition 2.5SiO$_2$: 1.0Al(OH)$_3$: 2.5KOH : 300H$_2$O.[46] Interestingly, the $Q^4(n\mathrm{Al})$ speciation of **CHA** prepared without using **FAU** was near the statistical average as shown in Fig. 3i and j. This indicates that the Al distribution of **CHA** derived from IZC is influenced by **FAU**.
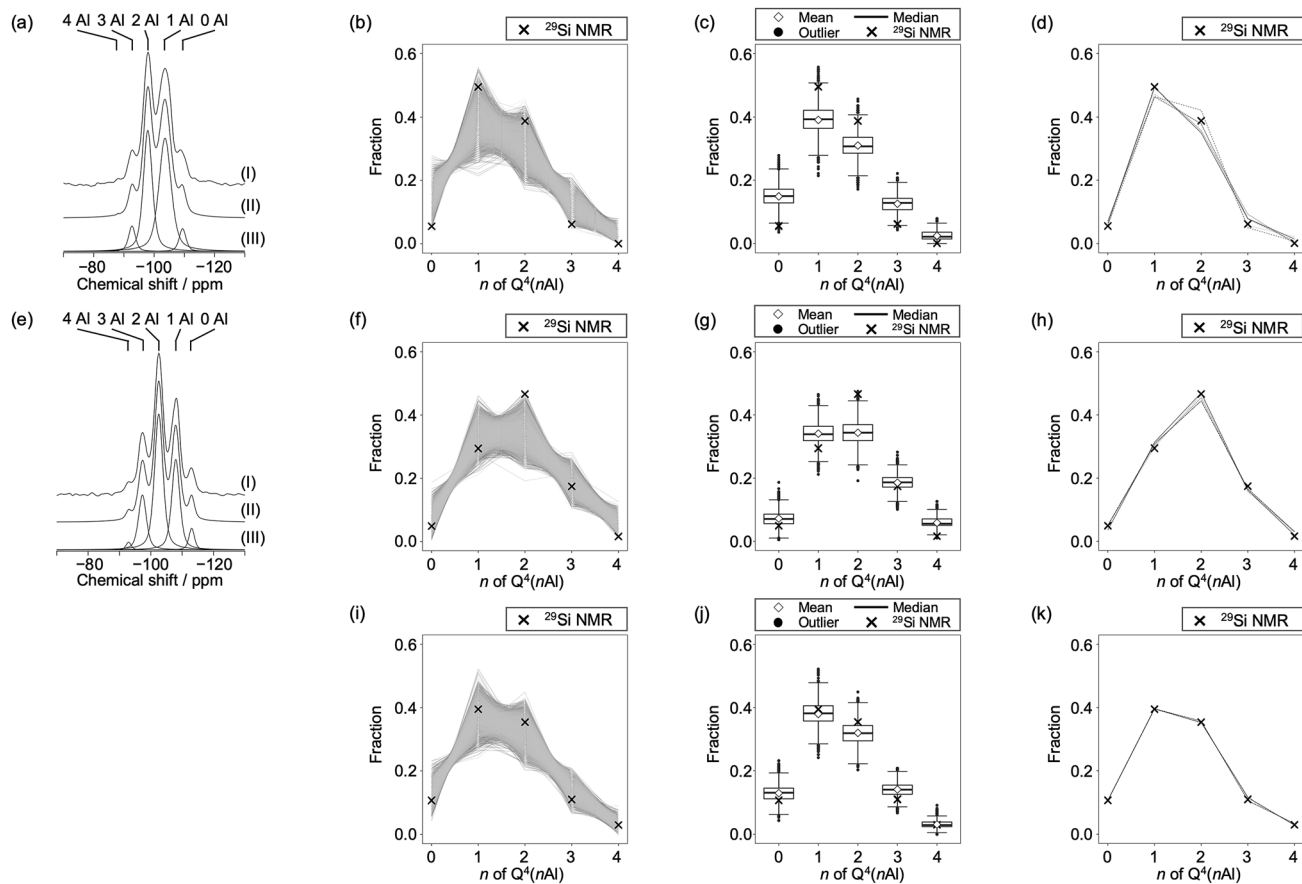
Fig. 3 ^{29}Si MAS NMR analyses combined with computational modeling for (a–d) the starting **FAU**, (e–h) **CHA** synthesized from **FAU**, and (i–k) **CHA** synthesized without using **FAU**. Note that the ^{29}Si MAS NMR spectrum of **CHA** synthesized without using **FAU** is not shown because data are taken from the literature.[46] (a) and (e) show ^{29}Si MAS NMR spectra of zeolites showing peaks derived from Si species coordinated with n O–Al bonds and $4 - n$ O–Si bonds where $n = 0, 1, 2, 3,$ and 4 for (I) observed, (II) simulated, and (III) deconvoluted spectra. (b), (f), and (i) show fractions of $Q^4(n\text{Al})$ species of 10 000 generated models with random atomic configurations as lines, together with the experimentally observed values as cross symbols. (c), (g), and (j) show box plots of the fractions of $Q^4(n\text{Al})$ species of 10 000 models with random atomic configurations. The top and the bottom of the box are the 75th and 25th percentiles, respectively. The bold bar inside the box indicates the median, while the diamond indicates the mean. The upper and lower bars are the most extreme data points within 1.5 times the interquartile range. Outliers are shown as black dots. Experimental values are shown as cross symbols. (d), (h), and (k) show the fractions of $Q^4(n\text{Al})$ Si species of the top five model structures (solid lines) that possess Si speciation closest to ^{29}Si NMR data (cross symbols).

To clarify the relationship between the Al distributions of **FAU** and **CHA**, we selected five models that are closest to the experimental $Q^4(n\text{Al})$ values as shown in Fig. 3d, h, and k. The crystal structures are shown in Fig. S3–S5.† To consistently analyze **FAU** and **CHA**, we focused on the atomic configuration of their common building unit, *d6r*. As previously reported,[23] there are only 19 topologically distinct atomic configurations for *d6r* as shown in Fig. 4, because Al–O–Al bonding is avoided in synthetic zeolites, which constitutes Löwenstein's rule.[47] As shown in Fig. 4, the starting **FAU** possessed *d6r* with three Al atoms (3Al), particularly 3Al-1, 3Al-2, and 3Al-3, as dominant species (see the first row in Fig. 5). After the **FAU**-to-**CHA** conversion, *d6r* with 2Al and *d6r* with 3Al decreased, while the fraction of *d6r* with 4Al increased, which is consistent with the decrease in Si/Al *via* the IZC. This result is significantly different from a hypothetical scheme in which **FAU** directly supplies *d6r* to crystallize **CHA**. It is likely that a more intensive rearrangement is involved, such as the formation of oligomers smaller than *d6r via* dissolution, and substitutions between Si and Al— a prism break.

As opposed to the view that IZC can proceed by selectively dissolving Si without mobilizing Al,[30] the current system likely involves mobile Al species owing to the highly alkaline conditions. Although the overall fraction of *d6r* with 4Al increased *via* the **FAU**-to-**CHA** conversion, the change in 4Al-1, 4Al-2, and 4Al-3 was relatively small. In the **CHA** derived from **FAU**, however, 4Al-4 and 4Al-5 markedly increased and were the dominant species. Among all *d6r* species with 4Al, 4Al-5 possesses the smallest number of Al–O–Si–O–Al moieties, which should be avoided as much as possible according to Dempsey's rule.[23,48] Because the Al–O–Al moiety is not allowed by Löwenstein's rule, 4Al-5 lacks a Si site that can be replaced with Al. Similarly, 4Al-4 disallows the substitution of Al for Si without violating Löwenstein's rule. Fig. 5 maps the relationships that would occur by isomorphically substituting Si with Al. While 4Al-4 and 4Al-5 are saturated with Al, the other species, namely, 4Al-1, 4Al-
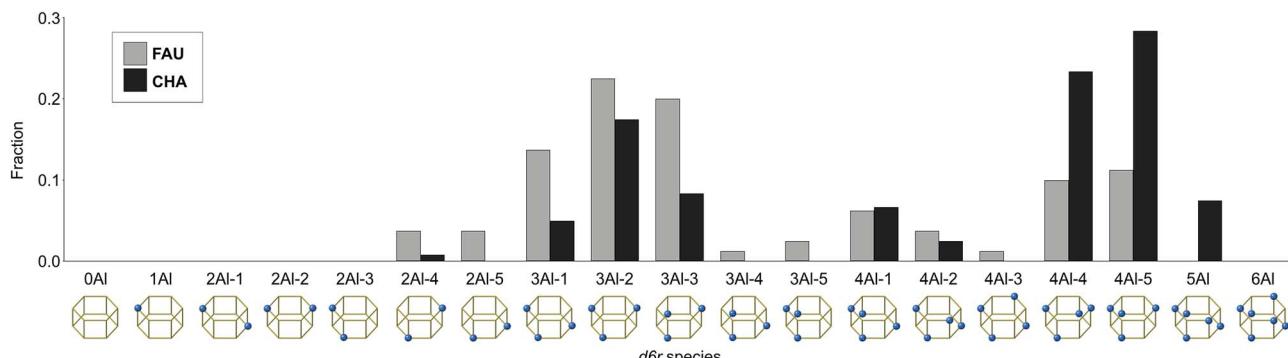
Fig. 4   Fractions and configurations of Al in the *d6r* units found in the starting **FAU** and resulting **CHA**.
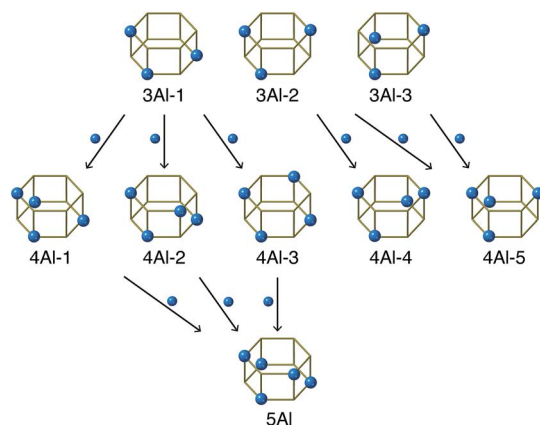

Fig. 5   Relationships between *d6r* species. The first row is the most abundant species in **FAU**; 3Al-1, 3Al-2, and 3Al-3. Arrows connect pairs of *d6r* species that can be transformed *via* isomorphic substitution between Si and Al. See Fig. S6† for complete relationships.

2, and 4Al-3, have replaceable Si sites, which can form *d6r* with 5Al directly (Fig. 5 and S6†). This could explain why only 4Al-4, 4Al-5, and 5Al significantly increased while 3Al-1, 3Al-2, and 3Al-3 decreased during the **FAU**-to-**CHA** conversion.

To confirm that these findings were not trends inherent in the current chemical composition, we compared the average abundance ratios of *d6r* species with the experimental results, and for randomly generated models with the same chemical compositions. The plot in Fig. S7† shows that 4Al-4, 4Al-5, and 3Al-2 are remarkably abundant in the models consistent with the experiments, confirming that the effects are likely derived from the specific Al distribution present in the synthesized **CHA**. Notably, the actual process of atomic rearrangement during the **FAU**-to-**CHA** conversion is likely to be more complicated than that shown in Fig. 5. Nevertheless, considering that **CHA** synthesized without using **FAU** had a random Al distribution (see Fig. 3j), it is reasonable to think that the Al distribution of the starting **FAU** influenced the resulting **CHA**.

Possible factors that can lead to such biased atomic configurations are charge balancing, the local environment of atoms, and energy stability.[21–23,25,38,49] To examine how energy stability affects the present system, we performed computational

modeling based on the crystal models obtained from ^{29}Si MAS NMR. The crystal models in Fig. S3–S5† lack the information of counter cations, which are potassium or sodium cations for the synthesis of the present **CHA** or the typical synthesis of **FAU**,[23] respectively. Brute-force modeling of all locations is feasible when the number of Al for each cell is small[50] but is unrealistic for the current Al-rich models with a myriad of possible combinations. Instead, we employed the Metropolis Monte-Carlo method[51] to obtain the location of counter cations within a reasonable amount of computational time. A cycle of the computational protocol starts with updating the location of cations and subsequently optimizing the structure. The application of this scheme for a **CHA** model consistent with ^{29}Si MAS NMR yielded the crystal structure shown in Fig. 6. As suggested in previous studies, the sites for potassium were the sites inside an eight-membered-ring and sites above *d6r*.[37,50] An identical computational protocol was applied for ten **CHA** models with the same chemical compositions but with random Al locations. As shown in Fig. 6c, **CHA** derived from **FAU** was energetically preferred with an energy difference of −328 kJ per mol per unit cell (U.C.) on average. On the other hand, the models consistent with **CHA** synthesized without **FAU** showed statistically similar energy to the counterparts with random Al locations (Fig. 6f).

Why did **CHA** synthesized from **FAU** have an energetically favorable, biased atomic configuration, while **FAU**-free synthesis produced **CHA** with random Al locations? Dusselier and Davis mentioned a low OH⁻ content, required for the successful crystallization of zeolites with even membered-rings, as a characteristic of IZC.[30] Conventional synthesis generally requires a high OH/Si ratio to promote the formation of zeolites with even membered-rings, but this could have been substituted with the 4 membered-ring, 6 membered-ring, and *d6r* found in **FAU** which could act as a substitute for the highly alkaline medium that favors even membered-rings.[30] Indeed, the synthesis of **CHA** by IZC requires less hydroxide (OH/Si = 0.82) than **FAU**-free synthesis (OH/Si = 1.0). When **FAU** was replaced with conventional Si and Al sources in an otherwise identical procedure, **CHA** did not crystallize, but formed a dense phase as shown in Fig. S8,† which implies that **FAU** influences formation pathways. The highly alkaline conditions in the **FAU**-free route may intensively dissociate and reunite Si–O and Al–O
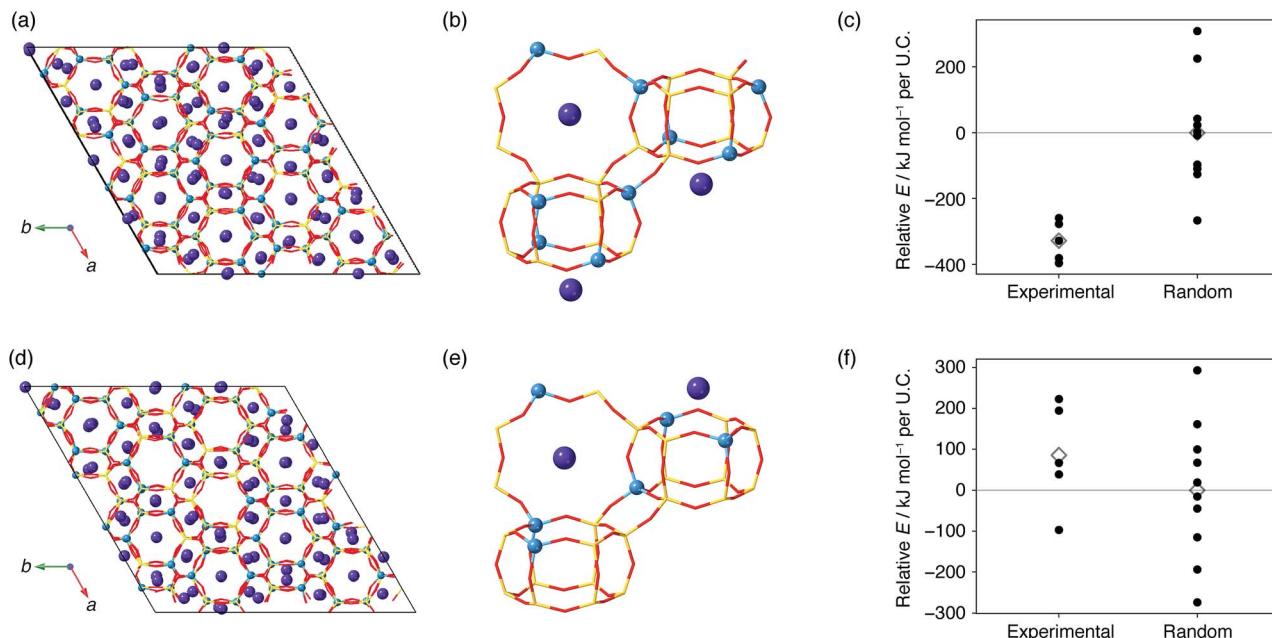
Fig. 6 Results of the Metropolis Monte-Carlo simulation for **CHA** synthesized from **FAU** (a–c) and **CHA** synthesized without using **FAU** (d–f).[46] (a), (b), (d), and (e) show the crystal structures derived from the Metropolis Monte-Carlo simulation of the models closest to ^{29}Si MAS NMR. Yellow sticks are Si atoms, red sticks are O atoms, light blue spheres are Al atoms, and purple spheres are K atoms. (c) and (f) show the framework energies of the final structures of the Metropolis Monte-Carlo simulation (closed circles) for the five models consistent with ^{29}Si MAS NMR and ten randomly selected models. Average energies are shown as open diamonds. Energies were offset by the average energy of models with random Al locations.
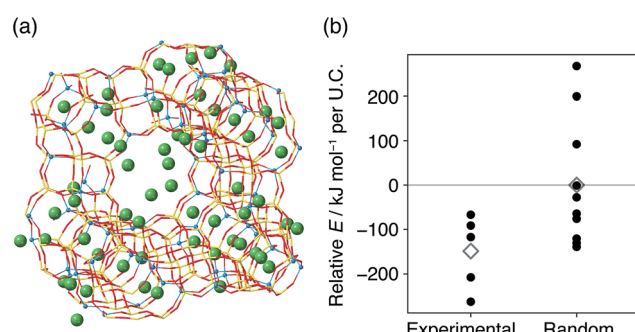
Fig. 7 (a) The crystal structure derived from the Metropolis Monte-Carlo simulation of the model closest to ^{29}Si MAS NMR of the starting **FAU**. Yellow sticks are Si atoms, red sticks are O atoms, light blue spheres are Al atoms, and green spheres are Na atoms. (b) Framework energies of the final structures of the Metropolis Monte-Carlo simulation (closed circles) for the five models consistent with ^{29}Si MAS NMR and ten randomly selected models. Average energies are shown as open diamonds. Energies were offset by the average energy of models with random Al locations.

bonds in starting materials to form monomers and very small oligomers that result in random atomic configurations, while lower alkalinity in the IZC route would maintain part of the atomic configurations of the starting **FAU** to construct **CHA** with spatially biased Al locations. This hypothesis should be confirmed by other characterization methods such as solution-state NMR techniques, which merits investigation in future work.

If the atomic configuration of **FAU** helps achieve a structure with low energy in the resulting **CHA**, it is natural to anticipate that the starting **FAU** also has an energetically stable Al distribution. To validate this hypothesis, we performed Metropolis Monte-Carlo analysis on **FAU** zeolite models. As shown in Fig. 7, the models consistent with the starting **FAU** showed more negative energies than the counterparts with random Al locations, which has also been reported for laboratory-prepared **FAU**.[23] Since detailed methods to reproduce commercial **FAU** have not been disclosed, it is of interest to investigate such laboratory-prepared **FAU** zeolites as starting materials in the future.

The findings reported here suggest that **CHA** synthesized *via* IZC can be energetically influenced by the atomic configuration of the starting **FAU**. A simple transfer of *d6r* cannot explain this phenomenon, which leads us to think that a more complicated breaking and reuniting of T–O bonds is involved. This reconstruction of aluminosilicate frameworks was not likely enough to completely depolymerize the energetically favorable atomic configuration in **FAU**, which could result in the crystallization of **CHA** with stable Al locations.

Conclusions

To the best of our knowledge, we performed the first end-to-end characterization of atomic configurations during **FAU**-to-**CHA** conversion. It is a relevant system for this purpose because both zeolites have only one tetrahedral site and are constructed with only *d6r*. Our synthesis employs **FAU** as the sole Si and Al source

and avoids amorphous matter formation. The results suggested that a specific rearrangement of silicates and aluminates occurred rather than a simple transfer of *d6r*. However, the atomic configuration of **CHA** was influenced by the starting **FAU**. Considering that the location of Al in the zeolite framework is essential for the most industrially important applications of **CHA**, namely, in methanol-to-olefin reactions and in the reduction of NO_x,[30,52–54] the atomic-level insight obtained in this study will contribute to the development of catalysts with improved performance. In addition, the approach used in this study which applies the spectroscopic technique and high-throughput computational modeling based on theoretical calculations would be applicable to other materials with complex formation mechanisms.

Conflicts of interest

There are no conflicts to declare.

Acknowledgements

References

1 S. Szymkuć, E. P. Gajewska, T. Klucznik, K. Molga, P. Dittwald, M. Startek, M. Bajczyk and B. A. Grzybowski, *Angew. Chem., Int. Ed.*, 2016, **55**, 5904–5937.

2 C. S. Diercks and O. M. Yaghi, *Science*, 2017, **355**, eaal1585.

3 M. B. Park, Y. Lee, A. Zheng, F.-S. Xiao, C. P. Nicholas, G. J. Lewis and S. B. Hong, *J. Am. Chem. Soc.*, 2013, **135**, 2248–2255.

4 M. E. Davis and R. F. Lobo, *Chem. Mater.*, 1992, **4**, 756–768.

5 T. M. Davis, T. O. Drews, H. Ramanan, C. He, J. Dong, H. Schnablegger, M. A. Katsoulakis, E. Kokkoli, A. V. McCormick, R. L. Penn and M. Tsapatsis, *Nat. Mater.*, 2006, **5**, 400–408.

6 V. P. Valtchev and K. N. Bozhilov, *J. Am. Chem. Soc.*, 2005, **127**, 16171–16177.

7 S. Mintova, N. H. Olson and T. Bein, *Angew. Chem., Int. Ed.*, 1999, **38**, 3201–3204.

8 R. Li, N. Linares, J. G. Sutjianto, A. Chawla, J. Garcia-Martinez and J. D. Rimer, *Angew. Chem., Int. Ed.*, 2018, **57**, 11283–11288.

9 A. I. Lupulescu and J. D. Rimer, *Science*, 2014, **344**, 729–732.

10 I. I. Ivanova, Y. G. Kolyagin, I. A. Kasyanov, A. V Yakimov, T. O. Bok and D. N. Zarubin, *Angew. Chem., Int. Ed.*, 2017, **56**, 15344–15347.

11 M. Khaleel, W. Xu, D. A. Lesch and M. Tsapatsis, *Chem. Mater.*, 2016, **28**, 4204–4213.

12 Q. Liu and A. Navrotsky, *Geochim. Cosmochim. Acta*, 2007, **71**, 2072–2078.

13 A. Aerts, C. E. A. Kirschhock and J. A. Martens, *Chem. Soc. Rev.*, 2010, **39**, 4626–4642.

14 S. Kumar, T. M. Davis, H. Ramanan, R. L. Penn and M. Tsapatsis, *J. Phys. Chem. B*, 2007, **111**, 3398–3403.

15 M. Kumar, M. K. Choudhary and J. D. Rimer, *Nat. Commun.*, 2018, **9**, 2129.

16 J. Dědeček, Z. Sobalík and B. Wichterlová, *Catal. Rev.*, 2012, **54**, 135–223.

17 R. Gounder and E. Iglesia, *J. Am. Chem. Soc.*, 2009, **131**, 1958–1971.

18 R. Gounder and E. Iglesia, *Acc. Chem. Res.*, 2012, **45**, 229–238.

19 J. Dedecek, M. J. Lucero, C. Li, F. Gao, P. Klein, M. Urbanova, Z. Tvaruzkova, P. Sazama and S. Sklenak, *J. Phys. Chem. C*, 2011, **115**, 11056–11064.

20 A. Vjunov, J. L. Fulton, T. Huthwelker, S. Pin, D. Mei, G. K. Schenter, N. Govind, D. M. Camaioni, J. Z. Hu and J. A. Lercher, *J. Am. Chem. Soc.*, 2014, **136**, 8296–8306.

21 T. Yokoi, H. Mochizuki, S. Namba, J. N. Kondo and T. Tatsumi, *J. Phys. Chem. C*, 2015, **119**, 15303–15315.

22 J. R. Di Iorio and R. Gounder, *Chem. Mater.*, 2016, **28**, 2236–2247.

23 M. D. Oleksiak, K. Muraoka, M. F. Hsieh, M. T. Conato, A. Shimojima, T. Okubo, W. Chaikittisilp and J. D. Rimer, *Angew. Chem., Int. Ed.*, 2017, **56**, 13366–13371.

24 B. C. Knott, C. T. Nimlos, D. J. Robichaud, M. R. Nimlos, S. Kim and R. Gounder, *ACS Catal.*, 2018, **8**, 770–784.

25 K. Muraoka, W. Chaikittisilp, Y. Yanaba, T. Yoshikawa and T. Okubo, *Angew. Chem., Int. Ed.*, 2018, **57**, 3742–3746.

26 J. E. Schmidt, L. Peng, J. D. Poplawsky and B. M. Weckhuysen, *Angew. Chem., Int. Ed.*, 2018, **57**, 10422–10435.

27 Y. Kamimura, W. Chaikittisilp, K. Itabashi, A. Shimojima and T. Okubo, *Chem.–Asian J.*, 2010, **5**, 2182–2191.

28 K. Itabashi, Y. Kamimura, K. Iyoki, A. Shimojima and T. Okubo, *J. Am. Chem. Soc.*, 2012, **134**, 11542–11549.

29 T. Ikuno, W. Chaikittisilp, Z. Liu, T. Iida, Y. Yanaba, T. Yoshikawa, S. Kohara, T. Wakihara and T. Okubo, *J. Am. Chem. Soc.*, 2015, **137**, 14533–14544.

30 M. Dusselier and M. E. Davis, *Chem. Rev.*, 2018, **118**, 5265–5329.

31 S. Goel, S. I. Zones and E. Iglesia, *Chem. Mater.*, 2015, **27**, 2056–2066.

32 M. Itakura, T. Inoue, A. Takahashi, T. Fujitani, Y. Oumi and T. Sano, *Chem. Lett.*, 2008, **37**, 908–909.

33 T. Sano, M. Itakura and M. Sadakane, *J. Jpn. Pet. Inst.*, 2013, **56**, 183–197.

34 N. Martín, M. Moliner and A. Corma, *Chem. Commun.*, 2015, **51**, 9965–9968.

35 C. Li, M. Moliner and A. Corma, *Angew. Chem., Int. Ed.*, 2018, **57**, 15330–15353.

36 D. Massiot, F. Fayon, M. Capron, I. King, S. Le Calvé, B. Alonso, J.-O. Durand, B. Bujoli, Z. Gan and G. Hoatson, *Magn. Reson. Chem.*, 2002, **40**, 70–76.

37 *Database of Zeolite Structures*, http://www.iza-structure.org/databases.

38 K. Muraoka, W. Chaikittisilp and T. Okubo, *J. Am. Chem. Soc.*, 2016, **138**, 6184–6193.

39 J. D. Gale and A. L. Rohl, *Mol. Simul.*, 2003, **29**, 291–341.

40 R. A. Jackson and C. R. A. Catlow, *Mol. Simul.*, 1988, **1**, 207–224.

41 C. Schroeder, M. R. Hansen and H. Koller, *Angew. Chem., Int. Ed.*, 2018, **57**, 14281–14285.

42 Y. Ji, M. A. Deimund, Y. Bhawe and M. E. Davis, *ACS Catal.*, 2015, **5**, 4456–4465.

43 R. M. Ravenelle, F. Schüßler, A. D'Amico, N. Danilina, J. A. van Bokhoven, J. A. Lercher, C. W. Jones and C. Sievers, *J. Phys. Chem. C*, 2010, **114**, 19582–19595.

44 M. Maldonado, M. D. Oleksiak, S. Chinta and J. D. Rimer, *J. Am. Chem. Soc.*, 2013, **135**, 2641–2652.

45 W. Qin, R. Jain, F. C. Robles Hernández and J. D. Rimer, *Chem.–Eur. J.*, 2019, **25**, 5893–5898.

46 D. E. Akporiaye, I. M. Dahl, H. B. Mostad and R. Wendelbo, *J. Phys. Chem.*, 1996, **100**, 4148–4153.

47 W. Lowenstein, *Am. Mineral.*, 1954, **39**, 92–96.

48 E. Dempsey, G. H. Kuehl and D. H. Olson, *J. Phys. Chem.*, 1969, **73**, 387–390.

49 Y. Román-Leshkov, M. Moliner and M. E. Davis, *J. Phys. Chem. C*, 2011, **115**, 1096–1102.

50 R. E. Fletcher, S. Ling and B. Slater, *Chem. Sci.*, 2017, **8**, 7483–7491.

51 N. Metropolis, A. W. Rosenbluth, M. N. Rosenbluth, A. H. Teller and E. Teller, *J. Chem. Phys.*, 1953, **21**, 1087–1092.

52 M. Yoshioka, T. Yokoi and T. Tatsumi, *ACS Catal.*, 2015, **5**, 4268–4275.

53 T. Nishitoba, N. Yoshida, J. N. Kondo and T. Yokoi, *Ind. Eng. Chem. Res.*, 2018, **57**, 3914–3922.

54 B. E. R. Snyder, M. L. Bols, R. A. Schoonheydt, B. F. Sels and E. I. Solomon, *Chem. Rev.*, 2018, **118**, 2718–2768.

55 C. Izutani, D. Fukagawa, M. Miyasita, M. Ito, N. Sugimura, R. Aoyama, T. Gotoh, T. Shibue, Y. Igarashi and H. Oshio, *J. Chem. Educ.*, 2016, **93**, 1667–1670.